Strong anisotropy and magnetostriction in the two-dimensional Stoner ferromagnet Fe_3GeTe_2

Houlong L. Zhuang,[1,2,*] P. R. C. Kent,[2,3] and Richard G. Hennig[4]

[1]*Department of Mechanical and Aerospace Engineering, Princeton University, Princeton, New Jersey 08544, USA*

[2]*Center for Nanophase Materials Sciences, Oak Ridge National Laboratory, Bethel Valley Road, Oak Ridge, Tennessee 37831, USA*

[3]*Computer Science and Mathematics Division, Oak Ridge National Laboratory, Bethel Valley Road, Oak Ridge, Tennessee 37831, USA*

[4]*Department of Materials Science and Engineering, University of Florida, Gainesville, Florida 32611, USA*

(Received 21 January 2016; revised manuscript received 8 March 2016; published 6 April 2016)

Computationally characterizing magnetic properies of novel two-dimensional (2D) materials serves as an important first step of exploring possible applications. Using density-functional theory, we show that single-layer Fe_3GeTe_2 is a potential 2D material with sufficiently low formation energy to be synthesized by mechanical exfoliation from the bulk phase with a van der Waals layered structure. In addition, we calculated the phonon dispersion demonstrating that single-layer Fe_3GeTe_2 is dynamically stable. Furthermore, we find that similar to the bulk phase, 2D Fe_3GeTe_2 exhibits a magnetic moment that originates from a Stoner instability. In contrast to other 2D materials, we find that single-layer Fe_3GeTe_2 exhibits a significant uniaxial magnetocrystalline anisotropy energy of 920 μeV per Fe atom originating from spin-orbit coupling. Finally, we show that applying biaxial tensile strains enhances the anisotropy energy, which reveals strong magnetostriction in single-layer Fe_3GeTe_2 with a sizable magneostrictive coefficient. Our results indicate that single-layer Fe_3GeTe_2 is potentially useful for magnetic storage applications.

DOI: 10.1103/PhysRevB.93.134407

I. INTRODUCTION

Two-dimensional (2D) materials such as graphene and MoS_2 exhibit a number of attractive properties that have been extensively studied in the past decade [1]. However, in contrast to mechanical and optoelectronic properties, the possibility of magnetism in 2D materials has received little attention. Most of thus far predicted 2D magnetic materials [2–11] are semiconductors with their magnetism originating from local magnetic moments and with exchange interactions that can be interpreted by the Heisenberg exchange model. In contrast, only a few metallic 2D materials exhibiting magnetic order have been computationally characterized [12,13]. Owing to the nature of itinerant electrons in a magnetic metallic 2D material, it is worthwhile investigating whether another classical model, namely, the Stoner model is applicable to understand the origin of the spontaneous magnetization.

In addition to this fundamental scientific question, ferromagnetic metallic single-layer materials hold great potential for magnetic storage applications. Modern magnetic storage media such as tape and hard disk commonly consists of ferromagnetic metallic thin films associated with high density of storage [14]. In essence, a 2D or single-layer material can be regarded as a thin film with ultrathin thickness. Therefore, applying single-layer materials for magnetic storage could further increase the density of data storage. A crucial parameter for magnetic recording materials is the magnetic anisotropy energy (MAE), which is defined as energy dependence on the direction of the magnetization. Generally, for storage applications materials with an easy magnetization axis and sizable MAE are desirable.

In this paper, we investigate using density-functional theory the magnetic properties of ferromagnetic single-layer Fe_3GeTe_2 (FGT), which is a prototype of ferromagnetic metallic single-layer material. The bulk Fe_3GeTe_2 compound was first synthesized by Deiseroth *et al.* in 2006 [15]. Figure 1 illustrates the structure of a single layer of the bulk compound. Although single-layer FGT has not yet been synthesized, we show that the layered bulk FGT compound exhibits a very weak van der Waals interaction between the layers, indicating the ease to mechanically exfoliate nanosheets from the bulk phase. We elucidate the origin of the ferromagnetic order and find that it can be described by Stoner's criterion. In addition, we determine that single-layer FGT exhibits a large MAE of 920 μeV per Fe atom. Finally, we explore the effect of strain on the MAE and demonstrate that applying tensile strains of 2% enhance the MAE by 50%. The dependence of the MAE on the strain shows strong magnetoelastic coupling in single-layer FGT, which exhibits a significant magnetostrictive coefficient.

II. METHODS

We perform density-functional calculations on single-layer and bulk FGT with the projector augmented wave (PAW) method [16,17], as implemented in the Vienna *ab initio* simulation package (VASP) [18,19] within the local density approximation (LDA) [20]. For bulk FGT, in addition to the LDA functional, we perform several comparison calculations utilizing the Perdew-Burke-Ernzerhof (PBE) [21] and the vdW-DF-optB88 [22–25] exchange-correlation functionals. The PAW potential describes the $1s^2 2s^2 2p^6$ states of Fe, the [Ne]$3s^2 3p^6 3d^{10}$ states of Ge, and the [Kr]$4d^{10}$ states of Te as core states. A plane wave basis set with a cutoff energy of 700 eV is used. The first Brillouin-zone integration is carried out using an $18 \times 18 \times 1$ and an $18 \times 18 \times 2$ Γ-centered Monkhorst-Pack grid for single-layer and bulk FGT, respectively. For all calculations a vacuum spacing of 16 Å sufficiently reduces the interlayer interactions due to the periodic boundary conditions. The atomic positions are fully optimized until the Hellman-Feynman forces on each atom are smaller than 0.01 eV/Å. To calculate the MAE, we include

*hzhuang@princeton.edu

 ©2016 American Physical Society

TABLE I. Lattice parameters (a_0 and c_0, in Å) and average magnetic moment per Fe atom (m, in units of the Bohr magneton μ_B) of bulk Fe_3GeTe_2 calculated with various exchange-correlation functionals. Available experimental data are shown for comparison. The lattice constants were measured from x-ray experiments and the magnetic moments were estimated via measuring the temperature-dependent magnetic susceptibility. The effective Hubbard U parameter ($U = 4.3$ eV) is adopted from Ref. [26], which determines the parameter based on unrestricted Hartree-Fock theory that is capable of removing self-interaction errors. Using different values for the U parameters, e.g., $U = 2.0$ or 6.0 eV, leads to a similar overestimation of the magnetic moment.

Methods	a_0	c_0	m
LDA	3.897	15.851	1.438
LDA+U	4.037	16.004	2.730
PBE	4.045	16.956	2.084
PBE+U	4.195	17.035	3.040
vdW-DF-optB88	4.045	16.539	2.057
vdW-DF-optB88+U	4.185	16.863	2.976
Experiment [27]	4.030	16.343	1.625
Experiment [15]	3.991	16.336	1.2

the spin-orbit coupling (SOC) in the computation with a full k-point grid, i.e., a total of 324 k points. The chosen energy cutoff and k-point meshes ensure the accuracy of the total energy, MAE, and magnetic moments to 0.1 meV/atom, 10 μeV/atom, and 0.001 μ_B/atom, respectively.

III. RESULTS AND DISCUSSION

We first assess the validity of applying the LDA functional to investigate bulk FGT, which crystallizes as a hexagonal layered structure with space group $P6_3/mmc$ (No. 194). Table I compares the calculated and measured [15,27] lattice parameters and magnetic moment in bulk FGT for several choices of exchange-correlation functionals. We observe that LDA slightly underestimates the lattice parameters by about 3%, which is common for a number of materials [28]. More importantly, LDA predicts the magnetic moment within the range of experimental values. Applying the Hubbard correction to the LDA functional with an effective U of 4.3 eV [26] for the Fe d states results in a slightly better agreement in the lattice parameters, however, the magnetic moment is drastically overestimated. The PBE functional, on the other hand, overestimates the lattice parameters and magnetic moment. Furthermore, including the U parameter into the PBE functional worsens the overestimation. Similarly, the vdW-DF-optB88 functional [22–25] and the vdW-DF-optB88+U method, which account for the interlayer van der Waals interactions, overestimate the lattice parameters and the magnetic moment. This suggests that the LDA functional alone is sufficient to accurately describe the structure and magnetic properties of bulk FGT. Given the good agreement between theory and experiment for bulk FGT, we expect that the LDA functional is also suitable to investigate the electronic and magnetic properties of single-layer FGT, which is the focus of this work. Henceforth, unless another method is mentioned, the LDA functional is used throughout our work.

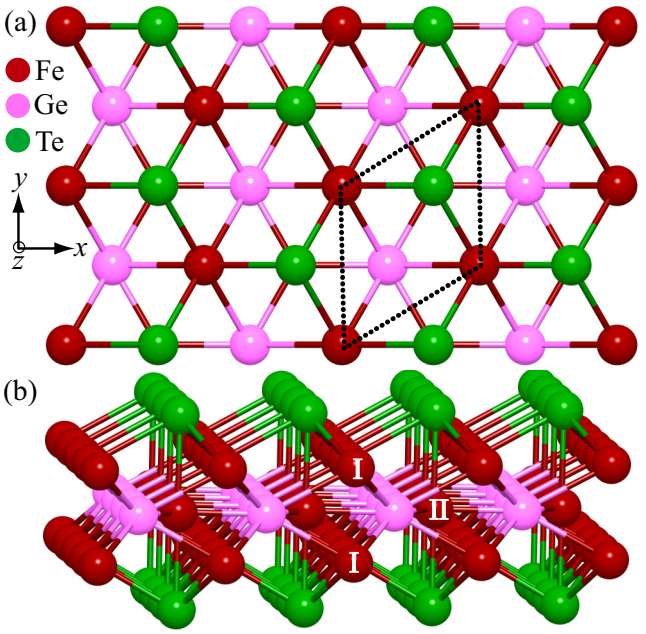

FIG. 1. (a) Top and (b) side views of the atomic structure of single-layer Fe_3GeTe_2. The unit cell is enclosed by the dotted lines. Inequivalent Fe sites are numbered by I and II, respectively.

Figure 1 illustrates the structure of single-layer FGT as one nanosheet of bulk FGT. The three Fe atoms in the unit cell are located in two inequivalent Wyckoff sites, henceforth referred to as Fe I and Fe II, respectively. Each unit cell consists of five sublayers, where the top and bottom layers are occupied by the Te atoms, the second and fourth layers by Fe I atoms, and the middle layer by both Fe II and Ge atoms.

We calculate the in-plane lattice parameter and local magnetic moments of the Fe I and Fe II atoms for single-layer FGT with the LDA functional. Table II shows that the lattice parameter of single-layer FGT is very close to the bulk value. Additionally, the average local magnetic moment of the Fe atoms, m_{avg}, in single-layer FGT is 1.48μ_B, which is nearly identical to that of bulk FGT.

We next examine the stability of single-layer FGT using the two criteria of (i) formation energy relative to the bulk phase and (ii) dynamically stable phonon modes [29,30]. The layered structure of bulk FGT suggests that a feasible experimental method to extract single-layer FGT sheets from bulk FGT could be mechanical or liquid exfoliation methods, which are widely used to obtain various single-layer materials such as graphene [31,32]. The easiness of exfoliating a layered material depends on the formation energy of single-layer

TABLE II. In-plane lattice parameter (a_0, in Å), individual and average magnetic moment of Fe I and Fe II atoms (m, in μ_B), and formation energy relative to the bulk phase (ΔE_f, in meV/atom) of single-layer Fe_3GeTe_2.The formation energy is calculated with both the LDA and the vdW-DF-optB88 functionals.

a_0	m_I	m_{II}	m_{avg}	ΔE_f^{LDA}	ΔE_f^{vdW}
3.909	1.723	1.005	1.484	48.9	62.8

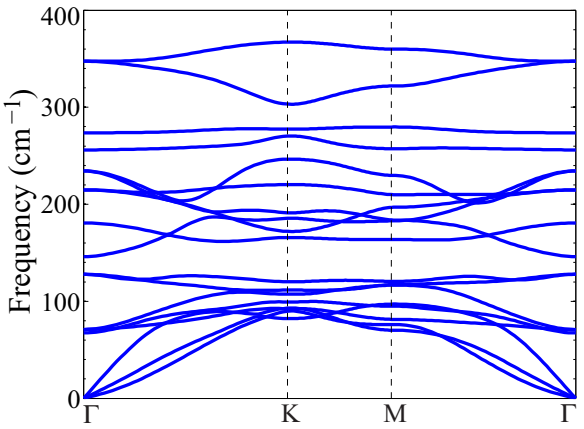

FIG. 2. The calculated phonon spectrum of single-layer Fe_3GeTe_2 with the DFT-LDA method.

sheets [33], which is defined as the energy difference between single-layer and bulk FGT [34,35].

Table II shows that the calculated formation energy, ΔE_f, of single-layer FGT relative to the bulk phase is merely 48.9 meV/atom (22.4 meV/Å^2) and 62.8 meV/atom (26.6 meV/Å^2) using the LDA and the vdW-DF-optB88 functional, respectively. Although the description of van der Waals interactions is inaccurate in the LDA functional, we observe similar binding energies for both functionals. The low formation energy is comparable to that of various 2D materials ranging from 5 to 40 meV/Å^2 as calculated using the nonlocal correlation functional method and the adiabatic-connection fluctuation-dissipation theorem within the random-phase approximation [36]. Further the ΔE_f of single-layer FGT is also well within the empirically observed bound of 200 meV/atom for the formation energy of 2D materials that have experimentally been synthesized as freestanding materials by, e.g., the exfoliation method, while 2D materials above that energy have only been synthesized as multilayers or on substrates [37,38]. Therefore, we predict that single-layer FGT can be obtained by exfoliation from bulk FGT.

Figure 2 shows the phonon spectrum of single-layer FGT. The lack of any unstable phonon modes suggests that single-layer FGT is dynamically stable. Hence single-layer FGT is a metastable phase with sufficiently low formation energy.

We proceed to investigate the electronic and magnetic properties of single-layer FGT. Figure 3 shows the spin and orbital projected band structure. Similar to its bulk counterpart, single-layer FGT remains metallic. We observe that the Fe $3d$ orbitals dominate the band structures around the Fermi level, with only minor hybridization with the Ge p and Te p states. Moreover, we observe several partially occupied d bands crossing the Fermi level, which is consistent with the resulting noninteger magnetic moment.

The metallic character, noninteger magnetic moment, and shift in the energy bands of single-layer FGT indicate that the ferromagnetism is of itinerant character. This suggests invoking the Stoner model rather than the Heisenberg model to understand the mechanism yielding the magnetic order, because the latter model is suitable to describe localized magnetic moments [39]. Within the Stoner model, two parameters determine whether a metal favors ferromagnetism or paramagnetism. The first one is the Stoner parameter I, and the second is the density of states at the Fermi level, $D(E_F)$, of the non-spin-polarized system. The former parameter describes the strength of electron exchange, whereas the latter is inversely proportional to the kinetic energy of the electrons. The competition between the exchange and kinetic energy are taken into account by the Stoner criterion, according to which ferromagnetism is adopted if $I D(E_F) > 1$.

The band dispersions for the two spin channels are quite similar, except that we observe a nearly rigid shift between the spin-up and spin-down bands surrounding the Fermi level, which is a typical feature of exchange splitting. The magnitude of exchange splitting at each k point is different, therefore we evaluate the average exchange splitting $\langle \epsilon_k \rangle$ for the two band structures [40] as the average difference of Kohn-Sham eigenvalues of the spin-up and spin-down bands and obtain $\langle \epsilon_k \rangle = 1.05$ eV. Using the relation $\langle \epsilon_k \rangle = I m_{avg}$, we obtain $I = 0.71$ eV for the Stoner parameter. Figure 3(c) shows that the calculated non-spin-polarized density of states at

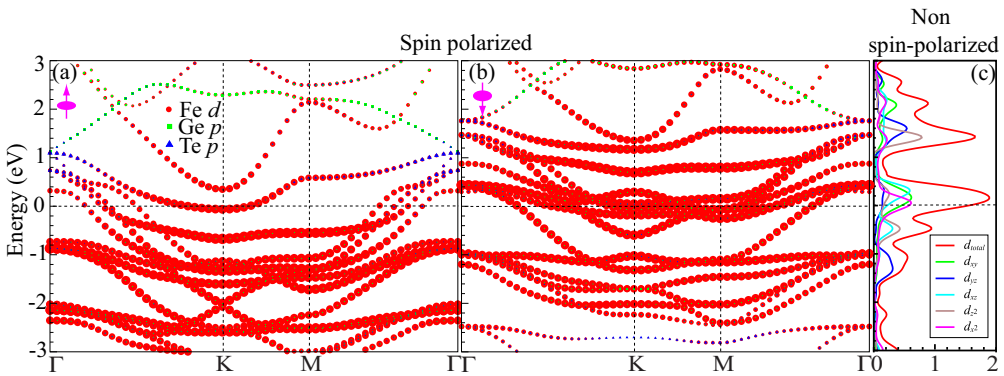

FIG. 3. Orbital-resolved (a) spin-up and (b) spin-down band structures of single-layer Fe_3GeTe_2. (c) Electronic density of states for the Fe d states in the non-spin-polarized system in units of states/eV/Fe atom/spin of single-layer Fe_3GeTe_2. This non-spin-polarized electronic structure is used to obtain the density of states at the Fermi level $D(E_F)$, which is one of the two Stoner parameters. All the band structures are from the DFT-LDA calculations.

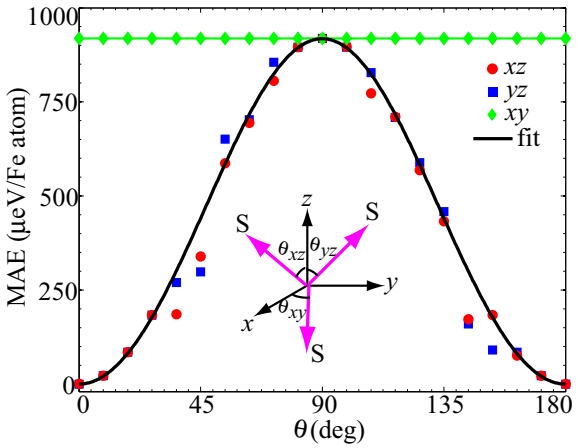

FIG. 4. Angular dependence of the magnetocrystalline anisotropy energy of single-layer Fe_3GeTe_2 with the direction of magnetization lying on three different planes. The energy, obtained from DFT-LDA calculations, is set to zero for the case of the spin being perpendicular to the 2D material. The inset illustrates that the spin vector S on the xz, yz, and xz plane is rotated with an angle θ about the y, x, and z axis, respectively.

the Fermi level is $D(E) = 1.56$ states/eV per Fe atom and spin. Therefore, Stoner's criterion that $ID(E) > 1$ is satisfied giving rise to the itinerant ferromagnetic order in single-layer FGT.

To explore potential applications of single-layer FGT in magnetic storage, we calculate its MAE. Figure 4 depicts the angular dependence of the MAE in the xz, yz, and xy planes. In the xz and yz plane the energy strongly depends on the direction of magnetization, whereas in the xy plane the energy is isotropic, consistent with the uniaxial anisotropy of the hexagonal structure. We observe that single-layer FGT exhibits an easy magnetization axis perpendicular to the 2D plane of the material. This agrees well with the experimental observations for the bulk FGT phase, where the easy magnetization axis points along the c lattice vector perpendicular to the layers of the material [15].

The presence of an easy magnetization axis in single-layer FGT affects the character of the magnetically ordered low-temperature phase. Recent calculations for another 2D material, VS_2, showed an easy plane for the magnetization [11] in contrast to the easy axis for single-layer FGT. As a result the magnetic ordering transitions differ between these 2D materials. The Mermin-Wagner theorem prohibits ferromagnetic order in 2D materials with continuous spin symmetries [41]. This means single-layer VS_2 can only display a quasi-long-range ordered phase at low temperatures with a power-law decay of the correlation function [42]. The easy magnetization axis in single-layer FGT, however, means that this material belongs to the family of 2D Ising magnets. A similar easy axis has also been reported in other single-layer ferromagnetic materials such as $CrX(X$=Si, Ge, and Sn)Te_3 [10].

Based on the hexagonal symmetry of single-layer FGT, the angular dependence of the MAE on the magnetization angle θ in the xz or yz plane can be fit to [43]

$$\mathrm{MAE}(\theta) = K_1 \sin^2\theta + K_2 \sin^4\theta, \tag{1}$$

where K_1 and K_2 are the magnetocrystalline anisotropy coefficients, and θ is measured relative to the easy axis. Figure 4 displays a good fit of Eq. (1) to the calculated MAE data. The resulting K_1 and K_2 are 0.844 and 0.074 meV/Fe atom, respectively. Both K_1 and K_2 are positive, which agrees with the fact that single-layer FGT exhibits a single easy axis.

We extract from Fig. 4 the uniaxial MAE defined as the energy difference of single-layer FGT with the magnetization axis aligned along the easy axis and perpendicular to it. The calculated MAE of single-layer FGT is 920 μeV/atom, which is significantly larger than the value for many ferromagnetic transition metals such as Fe, Co, and Ni with MAE typically in the order of μeV/atom [44]. In addition, the MAE of single-layer FGT is comparable to that of FeCo alloys (∼700–800 μeV/atom), which are predicted to be promising magnetic recording media [45]. The observed large MAE suggest that single-layer FGT has potential for applications in magnetic data storage applications.

The MAE can also be obtained from the force theorem, the validity of which has been proved by Freeman and co-workers [46]. According to the theorem, the MAE is calculated as

$$\mathrm{MAE} = \sum_{i,k}^{E_F} \epsilon_{ik|\theta=90^\circ} - \sum_{i,k}^{E_F} \epsilon_{ik|\theta=0^\circ}, \tag{2}$$

where the first and second terms denote the summation of the band energies ϵ_{ik} up to the Fermi level for the magnetic moments aligned in the $\theta = 90^\circ$ and 0° directions, respectively. The indices of bands and wave vectors are labeled by i and k, respectively. Using Eq. (2), we calculate the MAE of single-layer FGT as 520 μeV/Fe atom. Although this value is smaller than that from the torque method [47] as implemented in VASP, both MAE are indeed of the same magnitude. This confirms again the strong magnetic anisotropy in single-layer FGT.

In addition to the electronic contribution, the shape anisotropy caused by the dipole-dipole interactions also contributes to the MAE [48]. We denote the latter contribution by E_d, which can be written as [49]

$$E_d = \frac{1}{4\pi\mu_0} \sum_{qq'R} \frac{1}{|R+q-q'|^3} \left\{ M_q M_{q'} - 3\frac{[(R+q-q')M_q][(R+q-q')M_{q'}]}{|R+q-q'|^2} \right\}, \tag{3}$$

where μ_0 is the permeability of vacuum, R and q are the lattice vectors and atomic coordinates, respectively, and M refers to the magnetic moments. Since M_q and $M_{q'}$ are parallel to each other, $\Delta E_d = E_{d|\theta=90^\circ} - E_{d|\theta=0^\circ}$ is determined only by the second term of Eq. (3). The r^{-3} dependence defines the long-range nature of the dipole-dipole interactions. We therefore test the ΔE_d as a function of supercell sizes of $N \times N \times 1$, which is shown in Fig. 5. We find that the extrapolated ΔE_d for $N \to \infty$ is about -36 μeV/Fe atom, which is much smaller than the electronic contribution. Hence, the contribution of the shape anisotropy on the MAE of single-layer FGT can be neglected.

The significant MAE exhibited by single-layer FGT is caused by strong SOC. We calculate the total magnetic moment

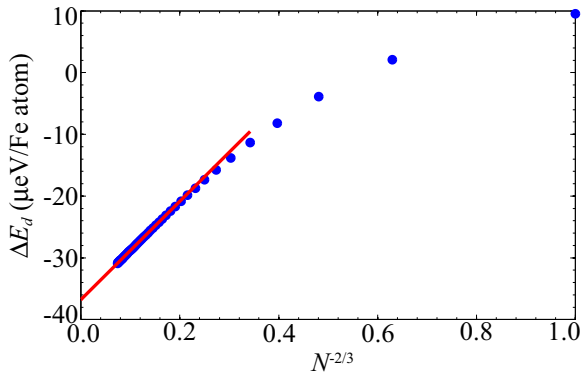

FIG. 5. Variation of shape anisotropy energy (blue dots) with the supercell size of single-layer FGT. An extrapolation of $N \to \infty$ is shown by the red solid line.

including SOC and find an average orbital moment for the Fe atoms of about $0.1\mu_B$. Although this value is much smaller than the orbital magnetic moment of an isolated Fe^{2+} ion of $2\mu_B$ according to Hund's second rule, the remaining orbital moment of the Fe ions in single-layer FGT is sizable, which indicates that the orbital motion is incompletely quenched and thus leads to the strong SOC and the large MAE. We also observe from Fig. 3(c) that the d_{xy} and $d_{x^2-y^2}$ atomic orbitals of Fe dominate the high density of state at the Fermi level that leads to the Stoner instability. In addition, the large orbital moment perpendicular to the plane of FGT may result in significant SOC and lead to the observed large MAE in single-layer FGT.

Strain has been shown to affect the MAE of various materials [50–53]. To explore the possibility to tune and further enhance the MAE of single-layer FGT, we apply biaxial strains to the material. Figure 6(a) depicts the calculated MAE as a function of strains ranging from −4% (compressive) to +4% (tensile). We observe that the MAE increases with increasing tensile strain. In particular, we observe a MAE of 1.59 meV/Fe atom for the maximum applied tensile strain of 4%. To understand the variation of MAE with strain, we show in Fig. 6(b) the total magnetic moment as a function of strains. We find that the total magnetic moment follows the same trend as the strain is varied. This suggests that the strength of SOC is enhanced by tensile strain leading to the increase of the MAE.

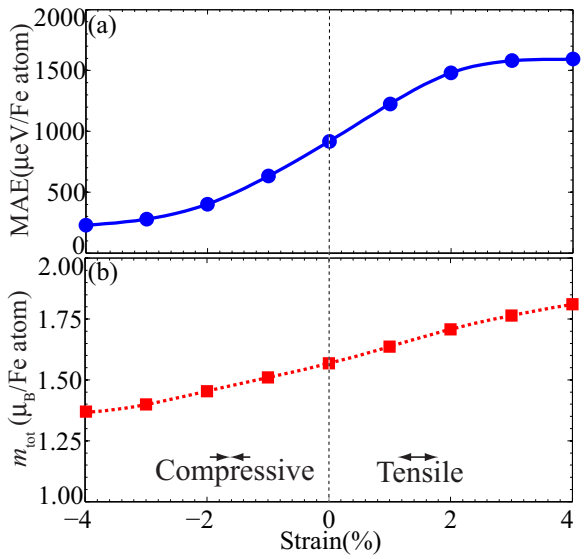

FIG. 6. Variation of (a) MAE and (b) total magnetic moment per Fe atom of single-layer Fe_3GeTe_2 under biaxial strain calculated using the DFT-LDA approach.

The dependence of the MAE on the applied biaxial strain reveals a strong magnetoelastic coupling that leads to magnetostriction [54] in ferromagnetic single-layer FGT. To determine the corresponding magnetostrictive coefficient λ, we write the general magnetoelastic energy density MAE of a hexagonal crystal as [55]

$$\begin{aligned} \mathrm{MAE} = {} & B_1\left(\alpha_3^2 - 1/3\right)(\epsilon_{11} + \epsilon_{22}) + B_2\left(\alpha_3^2 - 1/3\right)\epsilon_{33} \\ & + B_3\left[1/2\left(\alpha_1^2 - \alpha_2^2\right)(\epsilon_{11} - \epsilon_{22}) + \alpha_1\alpha_2\epsilon_{12}\right] \\ & + B_4(\alpha_3\alpha_1\epsilon_{31} + \alpha_2\alpha_3\epsilon_{23}). \end{aligned} \tag{4}$$

Here, B_i $(i = 1,2,3,4)$ are the magnetoelastic coupling coefficients [56] and α_j $(j = 1,2,3)$ are direction cosines of the magnetic moments relative to the easy axis. We focus on the 2D magnetostriction mode and apply biaxial strains $\epsilon_{11} = \epsilon_{22} = \epsilon$, while the other strain components are set to zero. In this case, $\alpha_3 = 1$ and $\alpha_1 = \alpha_2 = 0$, which reduces Eq. (4) to $\mathrm{MAE} = 4/3B_1\epsilon$. We evaluate the magnetoelastic coupling coefficient for biaxial strain as

$$B_1 = \frac{3}{4}\frac{d\mathrm{MAE}}{d\epsilon}, \tag{5}$$

and obtain a value of 27.5 meV/Fe atom or 0.075 J/m^2 by linear fitting the strain-dependent MAE shown in Fig. 6(a). With the calculated 2D elastic stiffness constant C_{11} of 134 N/m, we determine the magnetostrictive coefficient [57] $\lambda = -B_1/C_{11}$ as -559×10^{-6} or −559 ppm (parts per million). This value is sizable and comparable to those of $Fe_{1-x}Ga_x$ alloys (Galfenol) with a λ about 280 ppm [58], which indicates strong magnetostriction in single-layer FGT.

IV. CONCLUSIONS

We predicted using density-functional calculations that single-layer Fe_3GeTe_2 is a metastable metallic compound with a low formation energy and dynamically stable phonon modes. In addition, we observe a significant exchange splitting in the Fe d bands along with a high density of states at the Fermi level. Stoner's criterion is fulfilled leading to itinerant ferromagnetic order in this single-layer material. We show that single-layer Fe_3GeTe_2 exhibits significant magnetocrystalline anisotropy with an anisotropy energy of 920 μeV/atom that is tunable by mechanical strain. Finally, we find that single-layer Fe_3GeTe_2 possesses a substantial magnetostrictive coefficient of −556 ppm owing to strong magnetoelastic coupling. Our findings suggest that single-layer Fe_3GeTe_2 is a promising candidate suitable for magnetic storage applications. Furthermore, our process of characterizing this single-layer material including stability, exchange interactions, magnetocrystalline anisotropy, and tuning parameter serves as a general integral

procedure to search for other useful magnetic two-dimensional materials.

ACKNOWLEDGMENTS

This research was sponsored by the Laboratory Directed Research and Development Program (LDRD) of Oak Ridge National Laboratory, managed by UT-Battelle, LLC, for the U.S. Department of Energy. R.G.H. was supported by the NSF through CAREER award No. DMR-1056587. This research in part used computational resources of the Texas Advanced Computing Center under Contract No. TG-DMR140067. This research also used resources of the Oak Ridge Leadership Computing Facility at the Oak Ridge National Laboratory, which is supported by the Office of Science of the U.S. Department of Energy under Contract No. DE-AC05-00OR22725. We would like to thank Dr. Zheng Gai and Prof. David Mandrus for bringing Fe_3GeTe_2 to our attention.

This manuscript has been authored by UT-Battelle, LLC under Contract No. DE-AC05-00OR22725 with the U.S. Department of Energy. The United States Government retains and the publisher, by accepting the article for publication, acknowledges that the United States Government retains a nonexclusive, paid-up, irrevocable, worldwide license to publish or reproduce the published form of this manuscript, or allow others to do so, for United States Government purposes. The Department of Energy will provide public access to these results of federally sponsored research in accordance with the DOE Public Access Plan (http://energy.gov/downloads/doe-public-access-plan).

[1] J. Hu and R. Wu, Nano Lett. **14**, 1853 (2014).
[2] Z. Zhang, X. Zou, V. H. Crespi, and B. I. Yakobson, ACS Nano **7**, 10475 (2013).
[3] S. Tongay, S. S. Varnoosfaderani, B. R. Appleton, J. Wu, and A. F. Hebard, Appl. Phys. Lett. **101**, 123105 (2012).
[4] M. Kan, J. Zhou, Q. Sun, Y. Kawazoe, and P. Jena, J. Phys. Chem. Lett. **4**, 3382 (2013).
[5] M. Kan, S. Adhikari, and Q. Sun, Phys. Chem. Chem. Phys. **16**, 4990 (2014).
[6] J. Zhou and Q. Sun, J. Am. Chem. Soc. **133**, 15113 (2011).
[7] X. Li and J. Yang, J. Mater. Chem. C **2**, 7071 (2014).
[8] H. Zhang, L.-M. Liu, and W.-M. Lau, J. Mater. Chem. A **1**, 10821 (2013).
[9] S. Zhang, Y. Li, T. Zhao, and Q. Wang, Sci. Rep. **4**, 5241 (2014).
[10] H. L. Zhuang, Y. Xie, P. R. C. Kent, and P. Ganesh, Phys. Rev. B **92**, 035407 (2015).
[11] H. L. Zhuang and R. G. Hennig, Phys. Rev. B **93**, 054429 (2016).
[12] Y. Zhou, Z. Wang, P. Yang, X. Zu, L. Yang, X. Sun, and F. Gao, ACS Nano **6**, 9727 (2012).
[13] Y. Xu, X. Liu, and W. Guo, Nanoscale **6**, 12929 (2014).
[14] M. H. Kryder, Thin Solid Films **216**, 174 (1992).
[15] H.-J. Deiseroth, K. Aleksandrov, C. Reiner, L. Kienle, and R. K. Kremer, Eur. J. Inorg. Chem. **2006**, 1561 (2006).
[16] G. Kresse and D. Joubert, Phys. Rev. B **59**, 1758 (1999).
[17] P. E. Blöchl, Phys. Rev. B **50**, 17953 (1994).
[18] G. Kresse and J. Furthmüller, Phys. Rev. B **54**, 11169 (1996).
[19] G. Kresse and J. Hafner, Phys. Rev. B **47**, 558 (1993).
[20] J. P. Perdew and A. Zunger, Phys. Rev. B **23**, 5048 (1981).
[21] J. P. Perdew, K. Burke, and M. Ernzerhof, Phys. Rev. Lett. **77**, 3865 (1996).
[22] M. Dion, H. Rydberg, E. Schröder, D. C. Langreth, and B. I. Lundqvist, Phys. Rev. Lett. **92**, 246401 (2004).
[23] G. Román-Pérez and J. M. Soler, Phys. Rev. Lett. **103**, 096102 (2009).
[24] T. Thonhauser, V. R. Cooper, S. Li, A. Puzder, P. Hyldgaard, and D. C. Langreth, Phys. Rev. B **76**, 125112 (2007).
[25] J. Klimeš, D. R. Bowler, and A. Michaelides, J. Phys.: Condens. Matter **22**, 022201 (2010).
[26] N. J. Mosey, P. Liao, and E. A. Carter, J. Chem. Phys. **129**, 014103 (2008).
[27] B. Chen, J. Yang, H. Wang, M. Imai, H. Ohta, C. Michioka, K. Yoshimura, and M. Fang, J. Phys. Soc. Jpn. **82**, 124711 (2013).
[28] P. Haas, F. Tran, and P. Blaha, Phys. Rev. B **79**, 085104 (2009).
[29] H. L. Zhuang, A. K. Singh, and R. G. Hennig, Phys. Rev. B **87**, 165415 (2013).
[30] H. L. Zhuang, M. D. Johannes, M. N. Blonsky, and R. G. Hennig, Appl. Phys. Lett. **104**, 022116 (2014).
[31] K. S. Novoselov, D. Jiang, F. Schedin, T. J. Booth, V. V. Khotkevich, S. V. Morozov, and A. K. Geim, Proc. Natl. Acad. Sci. USA **102**, 10451 (2005).
[32] V. Nicolosi, M. Chhowalla, M. G. Kanatzidis, M. S. Strano, and J. N. Coleman, Science **340**, 1226419 (2013).
[33] G. Grimvall, B. Magyari-Köpe, V. Ozoliņš, and K. A. Persson, Rev. Mod. Phys. **84**, 945 (2012).
[34] H. L. Zhuang and R. G. Hennig, Appl. Phys. Lett. **101**, 153109 (2012).
[35] H. L. Zhuang and R. G. Hennig, JOM **66**, 366 (2014).
[36] T. Björkman, A. Gulans, A. V. Krasheninnikov, and R. M. Nieminen, Phys. Rev. Lett. **108**, 235502 (2012).
[37] A. K. Singh, K. Mathew, H. L. Zhuang, and R. G. Hennig, J. Phys. Chem. Lett. **6**, 1087 (2015).
[38] B. C. Revard, W. W. Tipton, A. Yesypenko, and R. G. Hennig, Phys. Rev. B **93**, 054117 (2016).
[39] S. Blundell, *Magnetism in Condensed Matter* (Oxford University Press, New York, 2001).
[40] J. Kubler, *Theory of Itinerant Electron Magnetism*, rev. ed. (Oxford University Press, New York, 2009).
[41] N. D. Mermin and H. Wagner, Phys. Rev. Lett. **17**, 1133 (1966).
[42] J. V. Jose, *40 Years of Berezinskii-Kosterlitz-Thouless Theory* (World Scientific, Singapore, 2013).
[43] R. C. O'Handley, *Modern Magnetic Materials: Principles and Applications*, 1st ed. (Wiley-Interscience, New York, 2006).
[44] S. V. Halilov, A. Y. Perlov, P. M. Oppeneer, A. N. Yaresko, and V. N. Antonov, Phys. Rev. B **57**, 9557 (1998).
[45] T. Burkert, L. Nordström, O. Eriksson, and O. Heinonen, Phys. Rev. Lett. **93**, 027203 (2004).
[46] X. Wang, D. Sheng Wang, R. Wu, and A. Freeman, J. Magn. Magn. Mater. **159**, 337 (1996).
[47] R. Wu and A. Freeman, J. Magn. Magn. Mater. **200**, 498 (1999).
[48] G. H. O. Daalderop, P. J. Kelly, and M. F. H. Schuurmans, Phys. Rev. B **41**, 11919 (1990).

[49] G. Y. Guo, J. Phys.: Condens. Matter **11**, 4329 (1999).
[50] Z. Torbatian, T. Ozaki, S. Tsuneyuki, and Y. Gohda, Appl. Phys. Lett. **104**, 242403 (2014).
[51] M. Sakamaki and K. Amemiya, Phys. Rev. B **87**, 014428 (2013).
[52] A. Boussendel, N. Baadji, A. Haroun, H. Dreyssé, and M. Alouani, Phys. Rev. B **81**, 184432 (2010).
[53] M. Costa, O. Grånäs, A. Bergman, P. Venezuela, P. Nordblad, M. Klintenberg, and O. Eriksson, Phys. Rev. B **86**, 085125 (2012).
[54] Y. Zhang, H. Wang, and R. Wu, Phys. Rev. B **86**, 224410 (2012).
[55] A. E. Clark and K. B. Hathaway, *Handbook of Giant Magnetostrictive Materials*, edited by G. Engdahl (Academic, San Diego, 2000), Chap. 1, pp. 1–48.
[56] M. Fähnle, M. Komelj, R. Q. Wu, and G. Y. Guo, Phys. Rev. B **65**, 144436 (2002).
[57] J. R. Cullen, Phys. Rev. B **52**, 57 (1995).
[58] H. Wang, Y. N. Zhang, R. Q. Wu, L. Z. Sun, D. S. Xu, and Z. D. Zhang, Sci. Rep. **3**, 3521 (2013).